The selenium isotopic variations in chondrites are mass-dependent; Implications for sulfide formation in the early solar system

Labidi, J., König, S., Kurzawa, T., Yierpan, A., Schoenberg, R.

Keywords

Early solar system, chondrites, sulfides, cosmochemistry, selenium isotopes

Abstract

Element transfer from the solar nebular gas to solids occurred either through direct condensation or via heterogeneous reactions between gaseous molecules and previously condensed solid matter. The precursors of altered sulfides observed in chondrites are for example attributed to reactions between gaseous hydrogen sulfide and metallic iron grains. The transfer of selenium to solids likely occurred through a similar pathway, allowing the formation of iron selenides concomitantly with sulfides. The formation rate of sulfide however remains difficult to assess. Here we investigate whether the Se isotopic composition of meteorites contributes to constrain sulfide formation during condensation stages of our solar system. We present high precision Se concentration and $\delta^{82/78}$Se data for 23 chondrites as well as the first $\delta^{74/78}$Se, $\delta^{76/78}$Se and $\delta^{77/78}$Se data for a sub-set of seven chondrites. We combine our dataset with previously published sulfur isotopic data and discuss aspects of sulfide formation for various types of chondrites.

Our Se concentration data are within uncertainty to literature values and are consistent with sulfides being the dominant selenium host in chondrites. Our overall average $\delta^{82/78}$Se value for chondrites is –0.21±0.43 ‰ (n=23, 2 s.d.), or -0.14±0.21 ‰ after exclusion of three weathered chondrites (n=20, 2 s.d.). These average values are within uncertainty indistinguishable from a previously published estimate. For the first time however, we resolve distinct $\delta^{82/78}$Se between ordinary (-0.14±0.07 ‰, n=9, 2 s.d.), enstatite (-0.27±0.05 ‰, n=3, 2 s.d.) and CI carbonaceous chondrites (-0.01±0.06 ‰, n=2, 2 s.d.). We also resolve a Se isotopic variability among CM carbonaceous chondrites. In addition, we report on $\delta^{74/78}$Se, $\delta^{76/78}$Se and $\delta^{77/78}$Se values determined for 7 chondrites. Our data allow evaluating the mass dependency of the $\delta^{82/78}$Se variations. Mass-independent deficits or excesses of ^{74}Se, ^{76}Se and ^{77}Se are calculated relative to the observed ^{82}Se/^{78}Se ratios, and were observed negligible. This rules out poor mixing of nucleosynthetic components to account for

the $\delta^{82/78}$Se variability and implies that the mass dependent Se isotopic variations were produced in a once-homogenous disk.

The mass-dependent isotopic difference between enstatite and ordinary chondrites may reflect the contribution of a kinetic sulfidation process at anomalously high H_2S-H_2Se contents in the region of enstatite chondrite formation. Experimental studies showed that high H_2S contents favor the formation of compact sulfide layers around metallic grains. This decreases the reactive surface, which tends to inhibit the continuation of the sulfidation reaction. Under these conditions sulfide growth likely occurs under isotopic disequilibrium and favors the trapping of light S and Se isotopes in solids; This hypothesis provides an explanation for our Se isotope as well as for previously published S isotope data. On the other hand, high $\delta^{82/78}$Se values in carbonaceous chondrites may result from sample heterogeneities generated by parent body aqueous alteration, or could reflect the contribution of ices carrying photo-processed Se from the outer solar system.

1- Introduction

Isotope variations among different classes of meteorites indicate that multiple sources have contributed to the origin of elements in the solar nebula. For example, mass independent isotopic signatures of chondrites for refractory elements such as chromium, zirconium or molybdenum ($T_{condensation}$ > 1300 K, (Lodders, 2003) reflect the contribution of multiple stellar sources to our proto-planetary disk (Dauphas, 2017; Trinquier et al., 2009). Various isotopic signatures across chondrite groups also imply that chromium, zirconium and molybdenum (and other refractory elements) were poorly mixed before their incorporation in solids (Dauphas, 2017 and references therein). On the other hand, bulk chondrites show negligible mass independent isotopic signatures for elements with lower condensation temperature such as iron, zinc, or silicon ($T_{condensation} \leq$ 1300 K) (Luck et al., 2005; Moynier et al., 2007; Savage and Moynier, 2013). This is remarkable since volatile elements were also provided by multiple stellar sources with mass-independent signatures (Bisterzo et al., 2011). The mass dependent patterns likely indicate that the more volatile elements have been homogenized in the proto-planetary disk before their relatively late condensation.

Nevertheless, chondrites display mass-dependent isotopic variations for moderately volatile elements (Luck et al., 2005; Moynier et al., 2007; Savage and Moynier, 2013). This requires isotopic

fractionations to occur after mixing in the nebular gas, or during condensation itself (Moynier et al. 2007). For instance, various chondrites groups show mass dependent zinc (Zn) isotopic variations. Zinc is carried in metals, sulfides and silicates, and since these phases have distinct Zn isotopic signatures, heterogeneous distribution (e.g. mineral sorting) can account for the isotope observation (Moynier et al. 2007). The mass dependent isotopic variations of the volatile element sulfur (S) is another example: enstatite chondrites show depletions of heavy S isotopes relative to ordinary chondrites (Defouilloy et al., 2016; Gao and Thiemens, 1993b). This observation, however, is still poorly understood since S in ordinary and enstatite chondrites is almost exclusively hosted in sulfides, ruling out inter-mineral fractionation or sorting to account for the observed S isotopic variations. In contrast to most other elements, sulfur is trapped in solids not through direct condensation of a cooling nebula, but via a heterogeneous reaction (i.e. reaction between gas and solids) between gaseous H_2S and iron grains in a given temperature range (between 700 and 500 K (Lauretta et al., 1996), following the reaction 1.

$$Fe^0+H_2S=FeS + H_2 \quad (1)$$

This so-called sulfidation reaction allowed the first iron sulfides to form (Zolensky and Thomas, 1995), although they likely underwent subsequent modification by parent body processes and/or chondrule formation (Rubin et al., 2007; Tachibana and Huss, 2005; Zanda et al., 1995). A turbulent nebula (Ciesla and Sandford, 2012) could allow the physical separation of sulfide and metal grains before their accretion in the meteorite parent bodies: This would provide fresh metal surfaces for further reaction with the residual H_2S reservoir, allowing the reaction 1 to occur as in a multitude of sulfidation events.

Thermodynamic data predict that selenium (Se) is trapped in solids via a heterogeneous reaction analogous to sulfidation: Gaseous H_2Se would react with metallic iron leading to the formation of iron selenides (Lodders, 2003) following reaction 2.

$$Fe^0+H_2Se=FeSe+H_2 \quad (2).$$

This reaction is predicted to be efficient over a similar temperature range than sulfidation (Lodders, 2003) which would lead selenides to be hosted in the sulfides (Dreibus et al., 1995). Here, we investigate the Se isotopic composition of chondrites and discuss whether the Se isotopic systematic combined with pre-existing S isotopic data can help describing the completion of reaction 1 and 2.

In the first report of Se isotope compositions of a range of undifferentiated meteorites, $\delta^{82/78}Se$ values were indistinguishable for the different chondrite groups within a 2 standard deviation (s.d.)

external reproducibility of ±0.37 ‰ (Vollstaedt et al., 2016). Here, we report $\delta^{82/78}$Se values for 23 bulk chondrites (H, L, LL, EL, EH, CO, CM, CV, and CI) and show that these objects display significant isotope variations outside our external reproducibility of ±0.10 ‰ (2 s.d.). We also report values for $\delta^{74/78}$Se, $\delta^{76/78}$Se and of $\delta^{77/78}$Se for a subset of seven bulk chondrites and show that the Se isotopic variations are mass dependent within external reproducibility for these ratios.

2. Analytical Techniques

2.1 Sample digestion and chemical purification of Se

The 23 chondrites investigated in this study cover a range of alteration, metamorphism and oxidation features (Table 1). The sample set includes nine observed falls and two hot-desert finds for carbonaceous chondrites, seven observed falls and two hot-desert finds for ordinary chondrites, two observed falls and one hot-desert find for enstatite chondrites (Table 1). Samples were obtained as chips from the interiors of the meteorites taken well away from the fusion crust to minimize the effects of terrestrial contamination and modification during atmospheric entry. Between 100 and 500 mg of rock chips were crushed and ground to powder in an agate mortar (Schoenberg and Blanckenburg, 2006; Schoenberg et al., 2016). About 5-50 mg of sample powder was weighed into quartz glass digestion tubes and digested in reverse aqua regia (3:1 HNO_3:HCl molar ratio) for 16 h at 220 °C and 100 bar in a high-pressure asher (Anton Paar^{TM}). For the determination of stable Se isotope ratios an adequate amount of our ^{74}Se-^{77}Se double spike was weighted into the glass tubes together with the sample powder to achieve sample-spike equilibration during sample digestion. No spike was added for sample aliquots on which potential mass-independent effects were to be determined. The procedural blanks associated with the glass vessels were roughly 1ng Se, which is insignificant compared to the amounts of sample Se ≥ 100 ng. For some samples, duplicates were digested in 5 ml of reverse aqua regia in closed teflon beakers placed on a hot plate for 24h at 100°C, where the procedural blanks were below detection limit (<0.1 ng Se).

After digestion, sample solutions were evaporated to dryness at 65 °C and further dried twice with 0.2ml 9 M HCl at 65 °C to ensure complete conversion of the residues to chloride form. Samples were then taken up in 4ml 6 M HCl and heated at 80°C for 2 hours to ensure quantitative conversion of Se^{6+} to Se^{4+} (Elwaer and Hintelmann, 2008; Pogge von Strandmann et al., 2014). Although solutions

120 can be purified with the thiol cotton fiber method (Elwaer and Hintelmann, 2008; Rouxel et al., 2002;
121 König et al., 2015), we followed a ion-exchange resin protocol recently developed (Kurzawa et al.,
122 2017). The solutions were loaded onto polypropylene columns containing 3 ml pre-cleaned Eichrom
123 AG1-X8 (100–200 mesh) anion resin. The pre-cleaning involved treatment with 8 ml 1 M HNO_3 and
124 4 ml high-purity water (18 MΩ cm) followed by conditioning the resin with 8 ml 6 M HCl. Se^{4+} does
125 not exchange with the resin and was directly collected during loading of the sample and elution of
126 additional 8 ml of 6 M HCl. Our approach allowed quantitative elimination of iron from the solutions
127 otherwise depressing the potential of hydride generation (see below and supplementary online
128 material). Sample solutions were then evaporated to dryness at 65 °C and dissolved in 1 ml 2 M HCl.
129 The solutions were then introduced to the MC-ICP-MS through a hydride generator which allows only
130 hydride-forming elements to be transported to the instrument plasma source.

131 **2.2. Mass spectrometry**

132 A detailed description of our instrumental setup, data treatment and correction is given in the
133 supplementary online file and in Kurzawa et al. (2017). Briefly, a CETAC HGX-200 hydride generator
134 was used as sample introduction system, where acidic sample solutions (in 2 M HCl) were mixed with
135 a reducing agent (0.2 M $NaBH_4$ in 0.05 M NaOH). This allowed the production of volatile H_2Se
136 hydrides transported through the hydride generator with a ca. 0.2 – 0.3 l/min Ar gas flow. The yields of
137 H_2Se formation were measured on both standard and sample solution: once processed, residual sample
138 solutions were collected from the excess liquid outlet of the hydride generator system and dried at 65
139 °C. They were subsequently taken up in 1 ml 2 M HCl and treated as a fresh sample in a measurement
140 session. For these solutions, signal intensities on the Neptune were always below detection limit,
141 implying yields of H_2Se formation in the first measurement to be roughly 100%. A ^{74}Se-^{77}Se enriched
142 tracer solution (~ 52 % ^{74}Se and ~ 47 % ^{77}Se, other Se isotopes accounting for < 1 %) previously
143 calibrated against a NIST SRM 3149 standard was used. The double spike deconvolution involved the
144 masses ^{74}Se, ^{77}Se, ^{78}Se and ^{82}Se. For each measurement session, a NIST SRM 3149 standard solution
145 was prepared with a 15 ng/ml Se concentration and sample analytes were diluted accordingly. At this
146 concentration the ^{82}Se voltage was 450-500 mV using a 10^{11} Ω resistor. Samples and standards were
147 measured for 40 cycles, each with an integration time of 4.194 seconds. Data is reported as relative per
148 mil difference to the international Se reference material NIST SRM 3149 in the δ-notation according to
149 equation 3:

$$\delta^{82/78}Se_{sample} = [(^{82/78}Se_{sample} / {}^{82/78}Se_{SRM3149}) -1] \times 1000 \quad (3)$$

At each double-spike measurement session, the NIST SRM 3149 standard and a Se in-house solution (MH-954) were measured to ensure reproducibility and accuracy. The average values and external reproducibility of $\delta^{82/78}$Se for NIST SRM 3149 and MH 954 during the course of this study were 0.00±0.06 ‰ (n=54) and -2.14±0.03 ‰ (n=7, both 2 s.d.), respectively. This is consistent with recently published values of MH-954 obtained via double-spike measurements of -2.23 ± 0.04 ‰ (Zhu et al., 2014) and -2.12±0.08‰ (2 s.d., n=100, Kurzawa et al. 2017).

For seven chondrites, a sample-standard bracketing approach was chosen to investigate the potential presence of mass-independent Se isotope effects. The bracketing standard was the NIST SRM 3149 solution. Complete removal of tracer memory from previous double spike Se runs was evaluated by monitoring the ^{77}Se/^{78}Se and ^{74}Se/^{78}Se ratios while the experimental apparatus was flushed with 2M HCl and (NIST) SRM 3149 solutions. Rinse out of spike memory took roughly three hours until Se isotopic ratios in the$^{74/78}$Se vs. $^{77/78}$Se space returned to the mass-dependent trajectory determined for unspiked NIST SRM 3149 standards. To enhance signal intensities on the minor isotopes ^{74}Se (~0.89 mol %), ^{76}Se (9.4 mol %) and ^{77}Se (~ 7.6 mol %), measurements were performed with solutions at a concentration of 50 ng/ml. At this concentration, measured signals at 10^{11} Ω resistance were 1300-1600 mV on ^{82}Se and 170-200 mV on ^{74}Se. Sample solutions were prepared to match the signal intensity of the standard within 10%. Samples and standards were measured for 100 cycles each with an integration time of 4.194 seconds. The in-house Se standard (MH-954) was repeatedly measured during measurement session (table 2) and yield average $\delta^{82/78}$Se of -2.11 ± 0.02 ‰ (2σ, n = 4, table 2) relative to the NIST SRM 3149 bracketing solution, which is indistinguishable from our double-spike estimate (-2.14±0.03‰, 2σ, n=7). Data for mass-independent isotope effects are reported as $\Delta^{n/78}$Se values (n is 77, 76 or 74), according to equation 4:

$$\Delta^{n}Se = \delta^{n/78}Se - 1000 * ((\delta^{82/78}Se/1000 + 1)^{\beta n} - 1) \quad (4)$$

The exponent β is the ratio of reduced isotope masses (Young et al., 2002), e.g. $\beta_{77} = (1/m_{78} - 1/m_{77})/(1/m_{78} - 1/m_{82})$=-0.2655.

3. Results

Selenium concentrations and isotopic composition of chondrites are given in tables 1 and 2. Note that for Se content and $\delta^{82/78}$Se values, uncertainty was taken as the external reproducibility obtained on repeated measurements of the shale standard SGR-1 (table 1). We obtain an average $\delta^{82/78}$Se of -0.11±0.09‰ (n=6, 2 s.d.) and a Se concentration of 3.5±0.5 ppm (n=6, 2 s.d.). Both Se isotopic composition and concentration are in agreement with the previously published value of -0.05±0.13‰ and 3.8±0.3 ppm (n=9, 2 s.d., Kurzawa et al. 2017, see also Pogge van Strandmann et al., 2014 and references therein). Note that all chondrite duplicates except Sahara 97072 yield a 2s.d. uncertainty better than 0.09‰ (Table 1). When no duplicates were measured, a conservative 0.09‰ external reproducibility determined for SGR-1 was used. For 7 chondrites, we performed conventional standard-sample bracketing measurements and determined values for Δ^{74}Se, Δ^{76}Se and Δ^{77}Se. Uncertainties are 1.50, 0.14 and 0.10 ‰ (2 s.d.), respectively.

3.1 Selenium concentrations

The average Se concentration obtained with the double-spike inversion for all carbonaceous chondrites studied here is 12±14 ppm (2s.d., n=11) whereas the average for falls only is 14±13 ppm (2s.d., n=9). Our CI meteorite samples Alais and Orgueil yield Se contents of 22±1 ppm and 21±1 ppm respectively, whereas the CM yield 13±1 ppm (Murchison) and 24±1 ppm (Mighei). Ornans and Lancé CO meteorites display homogeneous Se content of 8±1 ppm. In CV meteorites, Se contents range between 11±1 ppm Se (Mokoia) and 4±1 ppm Se (Axtell). When finds are excluded, the Se contents of CVs vary only between 11±1 ppm Se (Mokoia) and 9±1 ppm Se (Kaba). The only EH3 studied here, Sahara 97072, yields a Se content of 21±3 ppm Se (average of 3 duplicates), whereas Eagle and Atlanta, two EL6, yield Se contents of 10±1 and 9±1 ppm Se respectively. Ordinary chondrites show more restricted Se contents, with values ranging from 6±1 ppm for Dar Al Gani 298 (LL4) and 10±1 ppm for Borkut (L5) and Dhurmsala (LL6). The average Se content for all the ordinary chondrites is 8±3 ppm Se (n=9, 2 s.d.), whereas it is 9±2 ppm Se when only falls are considered (n=7, 2 s.d.).

For ordinary (OC), enstatite (EC) and carbonaceous chondrites (CC) no resolvable differences for Se concentrations were observed whether samples were digested at 100 or 220 °C (Table 1). Note

also that for all the chondrite classes analyzed here except Mighei, our data are consistent with previously reported Se contents in meteorites, whether data were acquired with neutron activation analysis (Dreibus et al. 1995) or wet chemistry followed by MC-ICP-MS measurements (Vollstaedt et al. 2016). This indicates that in contrast with earlier observations (Pogge von Strandmann et al. 2014), neither ashing at 220 °C nor hotplate digestion at 100 °C led to detectable Se losses.

3.2 Selenium content in carbonaceous chondrites matrices

In carbonaceous chondrites, the matrix is the main carrier of volatile elements and sulfides (Alexander et al., 2007; Bland et al., 2005; Huss et al., 2003; McSween and Richardson, 1977; Rubin et al., 2007). Hence, using literature data of matrix abundances in carbonaceous chondrites, we estimated the Se concentration in the matrices of our samples: We normalized the bulk Se contents $[Se]_{bulk}$ to matrix contents (McSween, 1977a, b; McSween and Richardson, 1977; Simon et al., 1995; Wasson et al., 2013; Zanda et al., 2006) to obtain Se contents in matrices $[Se]_{matrix}$. This approach was not extended to OC and EC since their chondrules contribute significantly to the volatile element budget of these meteorites (Alexander, 2005). As CIs consist of matrix alone, they show $[Se]_{bulk}=[Se]_{matrix}$ that we estimate at 21±1 ppm (n=2, 2 s.d.). For other CC falls, $[Se]_{matrix}$ range between 16±3 ppm (Kaba) and 40±3 ppm (Mighei). When these two samples are excluded, all $[Se]_{matrix}$ estimates are similar to the CI estimate, with values ranging between 19±4 ppm (Murchison) and 26±3 ppm (Mokoia), with an average of 22±5 ppm (n=7, 2 s.d.).

Note that we observe systematically lower [Se] for CV hot-desert finds relative to CV falls: Axtell displays a $[Se]_{bulk}$ of 4±1 ppm and $[Se]_{matrix}$ of 9±3 ppm Se. There is no available data for matrix content in Say al Uhaymir 085 but if the average matrix content in CV (44 vol%, Zanda et al. 2006) is used as a rough estimate, a concentration of 13 ppm Se is predicted for $[Se]_{matrix}$. Note that Kaba has a $[Se]_{matrix}$ of 16±3 ppm Se, somewhat lower than the average for CC (22±5, n=7, 2 s.d.).

Finally, we obtain 24±3 ppm Se for Mighei (2 s.d., n=4). This was duplicated using two independent digestion approaches (table 1). Mighei $[Se]_{bulk}$ value is significantly higher than the CM averages derived by Dreibus et al. (1995) of 13.5±2.8 ppm (n=10, 2 s.d.) or than the average of 12.9±1.5 ppm (n=2, 2 s.d.) by Vollstaedt et al. (2016). Our obtained Se content for Mighei is the highest reported so far for a CM and is within uncertainty indistinguishable from CI or EH chondrites.

3.3 Isotopic results

The $\delta^{82/78}$Se values range between –0.97±0.07‰ (Axtell, average of 2 duplicates, 2 s.d.) and +0.13±0.09‰ (Murchison, average of 5 duplicates, 2 s.d., Fig. 1) and average at -0.21±0.43‰ (n=23, 2 s.d.). Excluding 3 weathered chondrites (see below), the average is -0.14±0.21 ‰ (n=20, 2 s.d.). This is similar to the previous estimate of -0.20±0.26‰ (2 s.d., n=14, Vollstaedt et al. 2016). Although extending to lower values, our average for chondrites is within uncertainty to terrestrial silicate melt reference materials. Two studies provided data for basaltic reference materials and report average values of +0.36±0.22‰ (2 s.d., n=5, Rouxel et al. 2002) and +0.18±0.02‰ (2 s.d., n=1, Kurzawa et al. 2017). Dedicated studies are needed to address the relationship between the bulk silicate Earth and chondrites and to further assess terrestrial accretion scenarios using Se isotopes in addition to elemental Se systematics (Wang and Becker, 2013; König et al., 2014).

Ordinary chondrites show remarkably homogeneous $\delta^{82/78}$Se, with values ranging between -0.20±0.09‰ (Dar Al Gani 300, H3-5) and -0.09±0.06‰ (Bath, average of 3 duplicates, 2 s.d., Fig. 1). The average $\delta^{82/78}$Se for all ordinary chondrites is -0.14±0.07‰ (n=9, 2 s.d.). We observe no systematic variations of Se content or $\delta^{82/78}$Se between L, LL and H chondrites, or across various metamorphic grades of a given type. In addition, we observe no difference between falls and finds. For example, the hot desert find Dar Al Gani 300 (H3-5), with a Se concentration of 8±1 ppm Se and $\delta^{82/78}$Se of -0.20±0.09‰, is indistinguishable from all other OC sample.

Enstatite chondrites show homogeneous $\delta^{82/78}$Se values, with values ranging between -0.36±0.20‰ (Sahara 97072, EH3, 2 s.d.) and -0.24±0.09‰ (Eagle, EL6, Fig. 1). The average $\delta^{82/78}$Se for enstatite chondrites is -0.29±0.12‰ (n=3, 2 s.d.). Note that the value for Sahara 97072 is an average of two measurements obtained from two different digests. One is -0.29±0.09‰ (19±1 ppm Se), obtained at 220 °C (High-Pressure Asher digestion), whereas the duplicate digested at 100 °C (tabletop digestion) yields -0.43±0.09‰ (22±1 ppm Se, Table 1). The data are inconsistent with incomplete Se extraction at 100 °C, and the marginally distinct $\delta^{82/78}$Se values for Sahara 97072 duplicates could reflect sample heterogeneity. The average $\delta^{82/78}$Se for enstatite chondrites is -0.27±0.05‰ when only 220 °C digestions are included (n=3, 2 s.d.). We observe no significant variations of $\delta^{82/78}$Se values between EL6 (n=2) and EH3 (n=1, Fig. 1) or between EC falls and finds. This is the first report of distinct $\delta^{82/78}$Se values between EC and OC meteorites, EC displaying heavy Se isotope depletion relative to OC (Fig. 1).

Carbonaceous chondrites show the largest $\delta^{82/78}$Se range, with values between –0.97±0.07‰ (Axtell, average of 2 duplicates, 2 s.d.) and +0.13±0.09‰ (Murchison, average of 5 duplicates, 2 s.d.). The average $\delta^{82/78}$Se for all CC is -0.24±0.59‰ (2 s.d., n=11). The three CV Axtell, Say al Uhaymir 085 and Kaba with low Se contents also have the lowest $\delta^{82/78}$Se among carbonaceous chondrites and are not plotted in Fig. 1. As shown in Fig. 2, these chondrites show a positive correlation between $\delta^{82/78}$Se and $[Se]_{matrix}$, indicating Se loss during terrestrial weathering associated with an isotopic fractionation (section 4.2). Allende and Mokoia show less variable $\delta^{82/78}$Se values of -0.13±0.09‰ (Allende) and -0.20±0.09‰ (Mokoia). The average $\delta^{82/78}$Se value for these CVs is -0.17±0.08‰ (n=2, 2 s.d.). Excluding 3 weathered CV with low Se contents (fig. 2), the average estimate for carbonaceous chondrite is -0.12±0.30‰ (2 s.d., n=9). CV and CO (-0.14±0.06‰, n=2, 2 s.d.) falls remain indistinguishable from our OC estimate but we resolve relatively high $\delta^{82/78}$Se values in CI objects (-0.01±0.06‰, n=2, 2 s.d., Fig. 1) and heterogeneity among CM meteorites: Mighei yields a $\delta^{82/78}$Se of -0.20±0.07‰ (average of 4 replicates, 2 s.d.) similar to OC, whereas Murchison shows the highest $\delta^{82/78}$Se of our dataset: +0.13±0.07‰ (average of 5 replicates, 2 s.d., Fig. 1).

We present the first $\delta^{74/78}$Se, $\delta^{76/78}$Se, $\delta^{77/78}$Se and $\delta^{82/78}$Se values for chondrites via the use of standard-sample bracketing (Table 2). The low abundance of ^{74}Se leads to internal uncertainties for $\delta^{74/78}$Se to be ~ 1.5‰ (2 s.d., 2 s.e.m.=0.15‰). For $\delta^{76/78}$Se, $\delta^{77/78}$Se and $\delta^{82/78}$Se, internal uncertainties are 0.2% (2 s.d.) for standard and sample solutions. Over the measurement campaign, the Se solution MH-495 was used as an in-house standard. The solution was produced from the digestion of reagent-grade Se^0 pellets (Johnson et al., 1999). Our sample-standard bracketing measurements yield average $\delta^{82/78}$Se of -2.11 ± 0.02 ‰ (2σ, n = 4, table 2) versus the NIST SRM.3149 standard, which is indistinguishable from our double-spike value (-2.14±0.03‰, 2σ, n=7, see section 2.2) and from a recently published value obtained with the same double-spike procedure (-2.12±0.08‰, 2σ, n=100, Kurzawa et al.2017). In the absence of standards defining the Earth composition for Se isotopes, we here use the values of Δ^{74}Se, Δ^{76}Se and Δ^{77}Se of this well-characterized solution as an anchor for the Earth. Note that similarly to $\delta^{82/78}$Se, Δ^{74}Se, Δ^{76}Se and Δ^{77}Se data lie on the NIST SRM 3149 scale: by design, a value of 0.0‰ for Δ^{74}Se, Δ^{76}Se and/or Δ^{77}Se for a given sample reflects indistinguishable Se isotopic mass-dependence from the NIST SRM 3149 standard.

The average values of $\Delta^{74}Se$, $\Delta^{76}Se$ and $\Delta^{77}Se$ of the MH-495 solution (referred to as Earth standard in Fig. 4) are 0.0±0.1‰, -0.06±0.13‰ and 0.01±0.04‰ (all 2 s.d., n=4), respectively. This directly implies that the isotopic difference between MH-495 and NIST SRM 3149 (-2.11 ± 0.02 ‰ in $\delta^{82/78}Se$) follows strict mass-dependent laws for all the Se isotopic species. All the $\Delta^{74}Se$, $\Delta^{76}Se$ and $\Delta^{77}Se$ values for chondrites are found within uncertainty indistinguishable from MH-495 (fig. 4). For $\Delta^{74}Se$, values range between +1.3±1.5‰ (Ornans) and -0.7±1.5‰ (Mighei) and average at 0.3±1.5‰ (2 s.d., n=7). For $\Delta^{76}Se$, values range between +0.22±0.25‰ (Soko Banja) and -0.01±0.14‰ (Mighei) and average at +0.09±0.14‰ (2 s.d., n=7). For $\Delta^{77}Se$, values range between +0.27±0.30‰ (Soko Banja) and +0.04±0.10‰ (Murchison) and average at +0.12±0.15‰ (2 s.d., n=7). Data for both individual samples and chondrite averages overlap with terrestrial standards at 1 and 2 s.d. level. This is evidence that chondrites record mass-dependent Se isotopic signatures relative to both MH-495 and NIST SRM 3149. Although we report $\Delta^{74}Se$ data in table 2, our discussion is focused on $\Delta^{76}Se$ and $\Delta^{77}Se$. The $\Delta^{76}Se$ and $\Delta^{77}Se$ data remain statistically indistinguishable from our terrestrial standards but studies with lowered uncertainties and more various standards are needed to explore potentially subtle variations (Fig. 4).

4. Discussion

4.1 Sulfides as major host of Se in chondrites

Duplicated Se contents and $\delta^{82/78}Se$ are similar within uncertainty regardless of the amount of digested powder (ca. 5 - 50 mg, Table 1). For example, powders for aliquots Murchison 2 and 3 (both digested at 220 °C) weighed 12.9 and 33.1 mg, respectively. These aliquots yield 13±1 and 12±1 ppm Se and $\delta^{82/78}Se$ are 0.10±0.09‰ and 0.19±0.09‰, respectively (Table 1). In contrast, other heavy stable isotope systematics such as Si, Fe, Cu, Ni, and Zn only yield reproducible isotopic signatures for chondrites if more than 100 mg of sample powder are digested (e.g. Luck et al. 2005, Moynier et al. 2007). This is because multiple phases such as sulfides, metals, silicates and refractory inclusions host these respective elements. Our data support the idea that in contrast to other elements, Se is hosted in one phase only.

The acids used for digestion are a mixture of HNO_3 and HCl (reverse aqua regia, 3:1 HNO_3:HCl molar ratio) and no results presented here involved the use of hydrofluoric acid. The obtained Se concentrations are similar to results obtained with neutron activation analysis (Dreibus et

al. 1995). This indicates that the Se host phase in meteorites is quantitatively dissolved in acids at 100 C, without the use of hydrofluoric acid. Under these conditions, most silicates and oxides are refractory to quantitative digestion, whereas sulfides are readily dissolved (Burkhardt et al., 2012; Luck et al., 2005; Reisberg et al., 2009; Schönbächler et al., 2005). In addition, Vollstaedt et al. (2016) performed sequential Se extractions in chondrites involving a HF step. They showed that Se was not significantly associated with silicates. Taken together, available data indicate that Se is hosted in a sulfide phase.

4.2 Terrestrial weathering

Dreibus et al. (1995) compared Se contents of CC falls and finds. They observed significant Se depletions in hot-desert finds compared to falls that were interpreted as indication for terrestrial sulfide weathering under oxidizing conditions. Among our studied chondrites, Kaba is a highly weathered fall (Choi et al., 2000; Krot et al., 1998), whereas Say al Uhaymir 085 and Axtell are two hot-desert finds. These meteorites display low $[Se]_{matrix}$ ($\leq$ 16 ppm) compared to the CC average (22±5 ppm Se). In addition, the $\delta^{82/78}Se$ values of these chondrites are relatively low (<-0.4‰, Table 1) and positively correlated with $[Se]_{matrix}$ (Fig. 2). These data are consistent with Se loss during weathering. Further, the correlation observed in Fig. 2 is consistent with an isotopic fractionation associated with this Se loss. This would occur during oxidative weathering on Earth. The direction of the isotopic trend indicates preferential loss of isotopically heavy Se. Since light Se isotope would be preferentially lost during normal kinetic isotope fractionations (e.g. Young et al. 2002), our data rather indicate thermodynamic equilibrium. The data presented in Fig. 2 are best explained with an open-system Se loss that we could model assuming a Rayleigh distillation and a Se isotopic fractionation between fluid and rock $\Delta^{82/78}Se_{fluid\text{-}rock} = \delta^{82/78}Se_{fluid} - \delta^{82/78}Se_{rock}$ = 1.10‰ (Fig.2). This isotope fractionation was determined as the best fit of the data in Fig. 2.

Oxidation of selenides (Se^{2-}) to selenites (Se^{4+}) or selenates (Se^{6+}) could account for this isotopic fractionation. We note however that so far, all existing data indicate Se^{4+} or Se^{0} oxidation to Se^{6+} at T< 50 C to be associated with negligible isotope fractionations (Johnson, 2004). Only selenium reduction seems to be associated to significant isotope fractionations (1 to 5‰, Johnson, 2004). Based on this existing literature, a complex sequence of Se oxidation followed by partial reduction and re-precipitation could accounts for the data. However, evidence exists only for oxidative, not reductive, weathering of chondrites on Earth (Bland et al., 2006; Gounelle and Zolensky, 2001). Hence, Se

355 reduction is considered rather unlikely. Instead, we note that so far, the isotope fractionation during Se^{2-}
356 oxidation has not been investigated. It is thus conceivable that the ~ 1‰ fractionation required to
357 account for the variations seen in Fig. 2 illustrate a fractionation between selenide and oxidized Se
358 compounds. Theoretical or experimental studies on Se^{2-} oxidation and/or on sulfide weathering are
359 needed to further assess this scenario.

360 Two OC (Dar Al Gani 298, LL4, and Dar Al Gani 300, H3-5) and two EC (Sahara 97092,
361 EH3, and Atlanta, EL6) studied here are also hot-desert finds. These meteorites have 6±1 and 8±1 ppm
362 Se, respectively, in the range of other OC (average value of 8±3 ppm, n=9, 2 s.d., this study). The
363 $\delta^{82/78}$Se values of Dar Al Gani 298 (LL4) and Dar Al Gani 300, (H3-5) are -0.19±0.09‰ and -
364 0.20±0.09‰, respectively. These values are statistically indistinguishable from all other OC meteorites
365 analyzed here (Table 1). In contrast to the hot-desert CV finds, this argues against Se loss during
366 terrestrial weathering. This suggests that terrestrial weathering did not affect Se systematics of OC-EC
367 and CC similarly. Selenium in carbonaceous chondrites is mainly hosted in sulfides, themselves
368 occurring in the matrix (Bullock et al., 2005; Rubin et al., 2007). In contrast, sulfides in OC tend to
369 occur in chondrules (Zanda, 2004) and have been argued to significantly contribute to the Se budget in
370 OC (Alexander, 2005). We tentatively suggest that chondrules would have prevented significant
371 removal of Se from OC (and EC) meteorites, whereas the matrix sulfides in CC meteorites were
372 unshielded from terrestrial weathering.
373

374 **4.3 Varying kinetics of sulfide formation in the early solar system**

375 We resolve a $\delta^{82/78}$Se difference between ordinary and enstatite chondrites, with respective
376 average $\delta^{82/78}$Se values of -0.14±0.07‰ and -0.27±0.05‰ (Table 1). A student t-test was performed
377 between these two groups to evaluate the statistical significance of the $\delta^{82/78}$Se distinction. The
378 fractional probability that the two sets are identical is represented by a *P* value of 0.0003, indicating a
379 >99.9% probability that they represent different populations. The Δ^{76}Se and Δ^{77}Se values for Soko
380 Banja and Sahara 97072 remain indistinguishable from terrestrial standards (table 2), likely indicating
381 that Se isotopic variations between EC and OC are mass dependent. The stellar contributors to the Se
382 budget in the solar system carry mass independent isotope signatures (Bisterzo et al. 2011, see section
383 4.4). Observation of Se isotope mass dependent signatures (Fig. 4, Table 2) implies that the disk must
384 have been mixed, presumably while Se was in the gas phase. Mass dependent differences exist between

enstatite and ordinary chondrites for other, but not all isotopic systematics. For example, the Zn isotopic composition of type 3 EC and OC are indistinguishable (Moynier et al., 2007; Moynier et al., 2011). On the other hand, EC show mass dependent depletion of heavy S isotopes relative to OC (by ~0.3‰, Gao and Thiemens, 1993b). Our $\delta^{82/78}$Se averages for EC and OC are plotted against literature δ^{34}S values in figure S1, where the low $\delta^{82/78}$Se value for EC is shown to be associated to a low δ^{34}S value, relative to OC. Hence, it can be argued that similar to S, Se isotopic fractionation occurred concomitantly during sulfide formation.

One explanation involves the condensation of refractory sulfides in the region of enstatite chondrite formation. Exotic sulfides like oldhamites (CaS) are observed in EC (Kong and Ebihara, 1997; Larimer, 1968; Larimer and Ganapathy, 1987) and generally contribute between 1 to 10% of the bulk sulfide budget (DeFouilloy et al., 2016). These sulfides show 50% condensation temperatures > 1400 K (Lehner et al., 2013) whereas troilites are formed at temperatures between 700 and 500 K (Lauretta et al. 1996). In a cooling disk, oldhamites would therefore be formed before iron sulfides. If it is posited that oldhamites carry lower $^{34}S/^{32}S$ and $^{82}Se/^{78}Se$ ratios than iron sulfides, they could account for the relatively low $^{34}S/^{32}S$ and $^{82}Se/^{78}Se$ values observed in EC. However, the only available S isotope data on EC leachates indicate that oldhamite carry rather high $^{34}S/^{32}S$ ratios (DeFouilloy et al. 2016), consistent with oldhamites representing evaporative residues (Larimer and Ganapathy, 1987, DeFouilloy et al. 2016) after the sulfidation of ferroan silicates (Lehner et al. 2013). Unless oldhamites carry low $^{82}Se/^{78}Se$ (light Se) together with high $^{34}S/^{32}S$ ratios (heavy S), we rule out their contribution to explain the significantly low $\delta^{82/78}$Se values observed in EC.

Troilite evaporation would fractionate both $^{82}Se/^{78}Se$ and $^{34}S/^{32}S$ ratios: Troilite dissociation experiments leave residual troilite enriched in ^{34}S relative to evaporated S^0 (McEwing et al., 1980), consistent with the kinetic theory of gases (Richter and Davis, 2004). Troilite formed in the OC region could have experienced partially evaporation, or could have experienced more evaporation than sulfides in the EC forming region. This would preferentially enrich the OC sulfides in heavy isotopes (^{34}S and ^{82}Se) and could explain the observed isotopic difference between EC and OC for both S and Se isotope systematics. Chondrule formation could be the process responsible for the temperature increase above the evaporation point of troilite. However, this process would affect both OC and EC forming regions (Zanda, 2004), not accounting for any discrepancies between these meteorite groups.

Furthermore, chondrule formation has been shown to leave the $^{34}S/^{32}S$ ratio unchanged (Tachibana and Huss, 2005), inconsistent with the observations.

A plausible alternative is that Fe-sulfides were formed out of equilibrium in the EC forming region. In the solar system, iron sulfides are formed by Fe^0 sulfidation as in reaction 1, and Se is trapped in sulfides through the concomitant reaction 2 (Lauretta et al. 1996, Lodders, 2003). In contrast to direct condensation, reactions 1 and 2 are heterogeneous and kinetically inhibited below a temperature threshold (Lauretta et al. 1996, Lodders, 2003): at a solar H_2S/H_2 ratio (33×10^{-6}, Lodders, 2003), reaction 1 rate is maximum at ~ 700 K but remains significant down to ~ 500 K (Lauretta et al. 1996).

Lauretta et al. (1996) have shown that at a given Fe^0 grain size, increasing H_2S content have multiple impacts on the rate of reaction 1. At a H_2S/H_2 ratio of 33×10^{-5}, the temperature at which reaction 1 is maximum becomes ~ 850 K (Lauretta et al. 1996). More importantly, the rate decreases more rapidly with time as a result of compact sulfide layers forming around metal cores (Lauretta et al. 1996). As opposed to a linear kinetic regime at standard H_2S content, the reaction becomes driven by a parabolic kinetic behavior. The latter would lead to the preferential incorporation of light isotopes of both S and Se in sulfides, as predicted by the kinetic theory of gases (Richter and Davis, 2004). We suggest that the EC forming region was carrying a super-solar H_2S/H_2 ratio. If constant S/Se ratios of chondrites indicate constant H_2S/H_2Se ratios in the forming regions of OC and EC (Wang and Becker, 2013), the forming region of EC would be equally enriched in H_2Se. In such a H_2S-H_2Se rich nebular region, the non-linear kinetic regime of reactions 1 and 2 could have been triggered, leading to the preferential incorporation of light S and Se isotopes in EC sulfides. This would also account for the 0.15‰ and 0.30‰ depletions of the $^{82}Se/^{78}Se$ and $^{34}Se/^{32}Se$ ratios, respectively. While OC and EC forming regions would be both characterized with multiple/continuous sulfidation events, the H_2S-H_2Se enrichment in the EC forming region would produce the observed isotope disequilibrium. Note that independent observation from the EC trace element compositions tend to confirm that silicates and metals were exposed to an 'extreme sulfidizing environment' in the EC forming region, requiring a super-solar H_2S/H_2 ratio (Jacquet et al., 2015).

Considering H_2Se and H_2S and using the square root of molecules involved during condensation (Richter and Davis, 2004), first order estimates for the kinetic isotope fractionations of $^{82}Se/^{78}Se$ and $^{34}Se/^{32}Se$ ratios are ~25‰ and ~30‰ respectively. If these theoretical fractionations are

444 relevant to the early solar system, simple mass balance (assuming either open or closed system) require
445 less than 1% Se and S escaped sulfidation in the parabolic kinetic regime to account for the observed
446 0.15-0.30‰ isotope shift between EC and OC. Note however that during condensation, re-equilibration
447 processes lead theoretical fractionations closer to zero (Davis et al., 1990). These re-equilibration
448 processes tend to scale with the partial pressure of the element of interest in the gas phase and/or with
449 the total gas pressure (Richter and Davis, 2004). If similar re-equilibration processes are relevant to
450 reactions 1 and 2, the amount of S and Se escaping sulfidation could not be constrained without
451 experimental evidence, but would likely remain < 1%. Future experimental studies on S and Se isotopic
452 fractionations associated with reactions 1 and 2 will help to quantify the magnitude of isotope
453 fractionation (or re-equilibration, if any) as a function of the H_2S/H_2 and H_2Se/H_2 ratios in the gas
454 phase. This could provide quantitative constraints on the H_2S/H_2 and H_2Se/H_2 ratios of the EC forming
455 region.
456
457 **4.4. The case of CC meteorites: a contribution from the external solar system?**
458 We report on the Se content and isotopic composition of carbonaceous chondrites of the 4
459 main types (CI, CM, CV and CO, table 1). The Se content in CC matrices is constant across the types
460 investigated here (Fig. 3). This supports the idea of a CI-type matrix with a given Se content (22±5
461 ppm) distributed to CC asteroids and heterogeneously mixed with Se-depleted chondrules and
462 inclusions. Our observation contrasts with earlier reports (Bland et al. 2005) and rather supports the so-
463 called two component model (Alexander, 2005; Anders, 1964). According to this model, the budgets of
464 volatile elements in CCs are largely accounted for by volatile-rich matrices, whereas the contribution of
465 volatile-depleted chondrules and refractory inclusions is negligible. It is also noteworthy that our
466 samples span a range from highly altered chondrites (CI) to meteorites significantly less altered (CO
467 and CV). Constant Se concentration in matrices (Table 1, Fig. 3) argues for aqueous alteration on the
468 parent body to be a closed system for Se. This is consistent with chondrites altered on the parent body
469 (as opposed to terrestrial weathering) showing no evidence for losses of soluble elements when
470 compared to their unaltered counterpart (Bland et al., 2009). This was taken as evidence for closed
471 system aqueous alteration where silicates are hydrated and converted to phyllosilicates (Browning and
472 Bourcier, 1996; Rubin et al., 2007), but water flows are not significant enough to allow mobilization of
473 soluble elements (Na, Ca, and others, Bland et al. 2009). Note that Mighei shows anomalously high Se

content (Fig. 3). We tentatively explain the observation by sample heterogeneity in terms of sulfide distribution sampled by our allocated rock. An alternative possibility would be that this meteorite records an extra sulfidation event in the proto-planetary disk (e.g. reaction 1 and 2 pushed to completion). To our knowledge, the sulfur contents of this meteorite is unknown and needs to be determined in order to test the above hypotheses.

We derive $\delta^{82/78}$Se for CO (-0.14±0.06‰) and CV (-0.17±0.08‰) indistinguishable from OC meteorites. Δ^{74}Se, Δ^{76}Se and Δ^{77}Se values for these meteorites all remain indistinguishable from terrestrial standards (Fig. 4). On the other hand, CIs show a $\delta^{82/78}$Se of -0.01±0.06‰, distinct from OC. In addition, we resolve differences among CM meteorites: Mighei yields a $\delta^{82/78}$Se of -0.20±0.07‰ (average of 4 replicates, 2 s.d.) similar to the OC estimate, whereas Murchison shows the highest $\delta^{82/78}$Se of our dataset: +0.13±0.07‰ (average of 5 replicates, 2 s.d.). We here discuss the high $\delta^{82/78}$Se values observed in Orgueil, Alais and Murchison (Fig. 1).

The roughly constant $[Se]_{matrix}$ rules out alteration-derived fractionations. We concur with Vollstaedt et al. (2016) that parent body evaporation-condensation processes do not account for the Se isotopic composition of chondrites: Such processes would likely produce $\delta^{82/78}$Se variations correlated with $[Se]_{matrix}$ that are not observed (Fig. 3). A speculative heterogeneous distribution of phases (sulfides, metals, silicates, etc) is also ruled out, as Se is likely hosted only in sulfides (section 4.1). In principle, the Se isotopic variations could be attributed to the sampling of a poorly mixed disk after the injection of multiple nucleosynthetic components. Based on the astrophysical models discussed in Bisterzo et al. (2011), a 0.04% s-process deficit or 0.14% r-process excess sampled in Murchison relative to OC could account for the observed $\delta^{82/78}$Se difference between these objects. If correct, Δ^{76}Se and Δ^{77}Se of Murchison are predicted to be +0.25‰ and +0.33‰ according to the computation by Bisterzo et al. (2011). This is not observed; Our Murchison average over three digestions yields Δ^{76}Se and Δ^{77}Se values of +0.06±0.03‰ and +0.07±0.06‰ (2 s.d., n=3, Fig. 4), inconsistent with the above computation. The values are statistically indistinguishable from terrestrial standards (Fig. 4), confirming that the Se isotopic variations recorded in chondrites are strictly mass dependent within our uncertainty.

Chondrites of CI and CM types meteorites show evidence for more water interaction than other chondrites, indicating a higher contribution of ice water (Clayton and Mayeda, 1999). As observed for sulfur (Gao and Thiemens, 1993a), aqueous reactions could have generated partial

504 oxidation of Se. If an isotopic fractionation is associated with selenide oxidation (section 4.2) and if the
505 oxidation products and residues have distinct mobility, simple heterogeneous distribution of Se-bearing
506 phases could generate spatial Se isotopic variability. This idea would require that for CI and CM
507 objects, different pieces of a given meteorite would yield different Se isotopic composition. A similar
508 conclusion was reached to explain the variable S isotopic composition of Orgueil (Gao and Thiemens,
509 1993a).

510 An alternative possibility relies on the specificity of the reaction 2. If this reaction were
511 incomplete (as suggested for reaction 1, Labidi et al. 2017 and references therein), H_2Se would be left
512 in the gas phase of the disk at $T < 500$ K after the main sulfidation event(s). This molecule would
513 remain gaseous until the condensation of water ices at $T < 170$ K (Hoffmann and King, 2010; Irvine et
514 al., 2000). If this residual gas were carrying Se isotopic variations, its signature would be transferred to
515 the CI and CM during ice delivery (Clayton and Mayeda, 1999). One way to produce Se isotopic
516 heterogeneity in the residual gas is through photo-processing. It has been shown that H_2Se absorbs light
517 in the UV domain (Zhang et al., 2013). This gas can therefore be photodissociated by UV light emitted
518 by the young sun (Zahnle and Walker, 1982). Evidence exist that both ices and gases that they carry
519 have residual signatures resulting from UV irradiation (Ciesla and Sandford, 2012; Labidi et al., 2017).
520 H_2Se photodissociation by UV light may be associated to mass-dependent Se isotopic fractionations.
521 Similar with the photodissociation of H_2S under wavelengths higher than 200 nm (Farquhar et al.
522 2000), H_2Se photodissociation may generate a product and a residue carrying distinct Se isotopic
523 compositions with mass dependent signatures. The isotopically enriched H_2Se would have been
524 captured in icy components and subsequently transferred to the meteorite parent bodies through ice
525 accretion. Fluid/rock reactions would occur after ices melted, leading to parent body alteration (e.g.
526 Clayton and Mayeda, 1999). As required by S isotope data in carbonaceous chondrites (Labidi et al.
527 2017), the transfer of isotopically heavy Se to chondrite matrices would occur through the formation of
528 a second generation of sulfides: observations of the least altered CM meteorite Paris support the idea
529 that metal grains were available in the first alteration reactions (Hewins et al., 2014). Therefore, the
530 reactions 1 and 2 would also occur in solution on the parent body (Labidi et al. 2017), leading to the
531 formation of a second generation of sulfides. In this scenario, the icy-component would provide the
532 high $\delta^{82/78}$Se values to the secondary sulfides. Since our Se extraction protocol cannot distinguish

between the two generations of sulfides, the carbonaceous chondrites would display bulk Se with high $\delta^{82/78}$Se values relative to OC objects.

There are multiple possibilities to discriminate between Se isotopic heterogeneities generated by Se mobility during aqueous alteration or by sulfide formation after the contribution of H_2Se-bearing ices. Systematic studies on the Se isotopic compositions of Orgueil, Alais and Murchison are needed, to further investigate this hypothesis. This will be crucial to test whether alteration processes generated Se isotopic heterogeneities in these rocks. Photodissociation experiments on H_2Se will be essential to describe the latter hypothesis. If this process can produce the Se isotopic variations observed here, variations for Se isotope compositions of other carbonaceous chondrite could be used as a proxy of ice accretion to asteroids.

5. Conclusion

For the first time, we resolve $\delta^{82/78}$Se variations in chondrites. We show that OC (-0.14±0.07‰, n=9, 2 s.d.), EC (-0.27±0.05‰, n=3, 2 s.d.) and CI (-0.01±0.06‰, n=2, 2 s.d.) are distinct. In addition, whereas CO (-0.14±0.06‰, n=2, 2 s.d.) and CV (-0.17±0.08‰, n=2, 2 s.d.) remain indistinguishable from our OC estimate, we resolve heterogeneity among CM meteorites. Mighei yields $\delta^{82/78}$Se of -0.20±0.07‰ (average of 4 replicates, 2 s.d.) similar to the OC value, whereas Murchison shows the highest $\delta^{82/78}$Se of our dataset: +0.13±0.07‰ (average of 5 replicates, 2 s.d.). These $\delta^{82/78}$Se variations are associated with negligible Δ^{76}Se and Δ^{77}Se variations, indicating that chondrites display mass dependent Se isotopic signatures.

We observe no $\delta^{82/78}$Se variations as a function of metamorphism in OC samples, indicating that the Se isotope ratios remain constant throughout the heating processes experienced by asteroids. Only CC finds show evidence for Se isotope fractionation produced during terrestrial weathering, which we suggest is a consequence of Se being hosted in matrix sulfides, whereas it also occurs in chondrule-hosted sulfides in OC or EC samples.

The $\delta^{82/78}$Se differences in unweathered chondrites likely reflect the history of sulfide formation in the proto-planetary disk. The low $\delta^{82/78}$Se values in EC might reflect the contribution of a kinetic sulfidation process occurring under high H_2S-H_2Se content in the forming region of EC bodies. Our data will allow future experimental studies to quantify the amount of H_2S-H_2Se in the EC forming region. On the other hand, high $\delta^{82/78}$Se values in CC may reflect sample heterogeneities generated by

parent body alteration, or the contribution of ices carrying photo-dissociated Se from the outer solar system. Distinct predictions can be made for these two scenarios and further studies are needed to discriminate the proposed models.

Acknowledgements

This work was funded by an ERC Starting Grant (O_2RIGIN, 636808) to Stephan König. For generously supplying some of the samples the authors would like to thank the Musée d'Histoire Naturelle de Paris and U. Neumann (Department of Geosciences, University of Tuebingen). We thank Frederic Moynier for editorial handling, Dr. Philipp Pogge Von Strandmann and an anonymous reviewer for constructive comments.

Figure Captions

Fig. 1

$\delta^{82/76}$Se data obtained with the double spike technique. Uncertainty for individual measurements is 0.09‰, as the 2s.d. uncertainty for SGR-1 obtained here over 6 replicate measurements. The shaded area represents the average value ±2s.d. of the ordinary chondrite.

Fig. 2

The Se isotopic composition of CV chondrites plotted against $[Se]_{matrix}$. The positive trend is consistent with Se loss associated with isotopic fractionation during terrestrial weathering. The direction of the trend indicates that the heavy Se isotopes were preferentially lost. Isotope fractionation is here modelled under an open system loss of Se. The data are best fitted for a fractionation $\Delta^{82/78}Se_{fluid\text{-}rock} = \delta^{82/78}Se_{fluid} - \delta^{82/78}Se_{rock} = 1.10$‰, but acceptable values range between 0.55 and 1.50‰

Fig. 3

Values for $\delta^{82/78}$Se in unweathered carbonaceous chondrites plotted against $[Se]_{matrix}$. The constant $[Se]_{matrix}$ value is consistent with a model where budgets of volatile elements are largely accounted for by a volatile-rich matrix, whereas the contribution of volatile-depleted chondrules and refractory inclusions is negligible (the so-called two-component model, Anders 1964, Larimer and Anders 1967, 1970, Alexander 2005). Evaporation-condensation processes are ruled out to account for

593 the variable $\delta^{82/78}$Se values as they would likely produce $\delta^{82/78}$Se variations correlated with $[Se]_{matrix}$
594 that are not observed.
595
596 Fig. 4
597 Δ^{76}Se and Δ^{77}Se data obtained with the conventional sample-standard bracketing. Δ^{n}Se (n is 77, 76
598 or 74) is calculated as $\Delta^{n}Se = \delta^{n/78}Se - 1000((\delta^{82/78}S/1000 + 1)^{\beta} - 1)$. The exponent β is the ratio of
599 reduced isotope masses (Young et al. 2002). The shaded area represents the average value ±2s.d. of the
600 terrestrial standard MH-495.
601
602

603 Alexander, C.M.O.D., 2005. Re-examining the role of chondrules in producing the volatile element
604 fractionations in chondrites. Meteoritics & Planetary Science 40, 943-965.
605 Alexander, C.M.O.D., Fogel, M., Yabuta, H., Cody, G.D., 2007. The origin and evolution of chondrites
606 recorded in the elemental and isotopic compositions of their macromolecular organic matter. Geochim.
607 Cosmochim. Acta 71, 4380-4403.
608 Anders, E., 1964. Origin, age and composition of meteorites. Space Science Reviews 3, 583-714.
609 Bisterzo, S., Gallino, R., Straniero, O., Cristallo, S., Käppeler, F., 2011. The s-process in low-
610 metallicity stars - II. Interpretation of high-resolution spectroscopic observations with asymptotic giant
611 branch models. Monthly Notices of the Royal Astronomical Society 418, 284-319.
612 Bland, P., Zolensky, E.M., Benedix, G., Sephton, M., 2006. Weathering of chondritic meteorites.
613 Meteorites and the early solar system II 853-867.
614 Bland, P.A., Alard, O., Benedix, G.K., Kearsley, A.T., Menzies, O.N., Watt, L.E., Rogers, N.W., 2005.
615 Volatile fractionations in the early Solar System and chondrule/matrix complimentarity. Proceedings of
616 the National Academy of Sciences 102, 13755-13760.
617 Bland, P.A., Jackson, M.D., Coker, R.F., Cohen, B.A., Webber, J.B.W., Lee, M.R., Duffy, C.M.,
618 Chater, R.J., Ardakani, M.G., McPhail, D.S., McComb, D.W., Benedix, G.K., 2009. Why aqueous
619 alteration in asteroids was isochemical: High porosity≠high permeability. Earth and Planetary Science
620 Letters 287, 559-568.
621 Browning, L., Bourcier, W., 1996. Fluid Conditions During the Alteration of CM Chondrites.
622 Meteoritics & Planetary Science 31, A22.
623 Bullock, E.S., Gounelle, M., Lauretta, D.S., Grady, M.M., Russell, S.S., 2005. Mineralogy and texture
624 of Fe-Ni sulfides in CI1 chondrites: Clues to the extent of aqueous alteration on the CI1 parent body.
625 Geochimica et Cosmochimica Acta 69, 2687-2700.
626 Burkhardt, C., Kleine, T., Dauphas, N., Wieler, R., 2012. Origin of isotopic heterogeneity in the solar
627 nebula by thermal processing and mixing of nebular dust. Earth and Planetary Science Letters 357-358,
628 298-307.
629 Choi, B.-G., Krot, A.N., Wasson, J.T., 2000. Oxygen-isotopes in magnetite and fayalite in CV
630 chondrites Kaba and Mokoia. Meteoritics and Planetary Science 35, 1239-1248.
631 Ciesla, F.J., Sandford, S.A., 2012. Organic synthesis via irradiation and warming of ice grains in the
632 solar nebula. Science 336, 452-454.
633 Clayton, R.N., Mayeda, T.K., 1999. Oxygen isotope studies of carbonaceous chondrites. Geochimica et
634 Cosmochimica Acta 63, 2089-2104.
635 Dauphas, N., 2017. The isotopic nature of the Earth's accreting material through time. Nature 541, 521-
636 524.
637 Davis, A.M., Hashimoto, A., Clayton, R.N., Mayeda, T.K., 1990. Isotope mass fractionation during
638 evaporation of Mg2SiO4. Nature 347, 655-658.
639 Defouilloy, C., Cartigny, P., Assayag, N., Moynier, F., Barrat, J.A., 2016. High-precision sulfur isotope
640 composition of enstatite meteorites and implications of the formation and evolution of their parent
641 bodies. Geochimica et Cosmochimica Acta 172, 393-409.

Dreibus, G., Palme, H., Spettel, B., Zipfel, J., Wanke, H., 1995. Sulfur and selenium in chondritic meteorites. Meteoritics 30, 439-445.
Elwaer, N., Hintelmann, H., 2008. Selective separation of selenium (IV) by thiol cellulose powder and subsequent selenium isotope ratio determination using multicollector inductively coupled plasma mass spectrometry. Journal of Analytical Atomic Spectrometry 23, 733-743.
Gao, X., Thiemens, M.H., 1993a. Isotopic composition and concentration of sulfur in carbonaceous chondrites. Geochimica et Cosmochimica Acta 57, 3159-3170.
Gao, X., Thiemens, M.H., 1993b. Variations of the isotopic composition of sulfur in enstatite and ordinary chondrites. Geochimica et Cosmochimica Acta 57, 3171-3176.
Gounelle, M., Zolensky, M.E., 2001. A terrestrial origin for sulphate veins in CI1 chondrites. Meteorit Planet Sci 36.
Hewins, R.H., Bourot-Denise, M., Zanda, B., Leroux, H., Barrat, J.-A., Humayun, M., Göpel, C., Greenwood, R.C., Franchi, I.A., Pont, S., Lorand, J.-P., Cournède, C., Gattacceca, J., Rochette, P., Kuga, M., Marrocchi, Y., Marty, B., 2014. The Paris meteorite, the least altered CM chondrite so far. Geochimica et Cosmochimica Acta 124, 190-222.
Hoffmann, J.e., King, M.G., 2010. Selenium and selenium coumpounds. Encyclopedia of Chemical Technology, 1-36.
Huss, G.R., Meshik, A.P., Smith, J.B., Hohenberg, C.M., 2003. Presolar diamond, silicon carbide, and graphite in carbonaceous chondrites: Implications for thermal processing in the solar nebula. Geochimica et Cosmochimica Acta 67, 4823-4848.
Irvine, W.M., Schloerb, F.P., Crovisier, J., Fegley Jr, B., Mumma, M.J., 2000. Comets: A link between interstellar and nebular chemistry. Protostars and Planets IV V. Mannings, A. P. Boss, and S. S. Russell, Eds. University of Arizona Press., 1159-1200.
Jacquet, E., Alard, O., Gounelle, M., 2015. The formation conditions of enstatite chondrites: Insights from trace element geochemistry of olivine-bearing chondrules in Sahara 97096 (EH3). Meteoritics and Planetary Science 50, 1624–1642.
Johnson, T.M., 2004. A review of mass-dependent fractionation of selenium isotopes and implications for other heavy stable isotopes. Chemical Geology 204, 201-214.
Johnson, T.M., Herbel, M., Bullen, T., Zawilanski, P., 1999. Selenium isotope ratios as indicators of selenium sources and oxyanion reduction. Geochim Cosmochim Acta 63, 2775–2783.
Kong, P., Ebihara, M., 1997. The origin and nebular history of the metal phase of ordinary chondrites. Geochimica et Cosmochimica Acta 61, 2317-2329.
König, S., Lorand, J.-P., Luguet, A., Pearson, D.G., 2014. A non-primitive origin of near-chondritic S–Se–Te ratios in mantle peridotites; implications for the Earth's late accretionary history. Earth and Planetary Science Letters, 385: 110-121.
König, S., Lissner, M., Lorand, J.-P., Bragagni, A., Luguet, A., 2015. Mineralogical control of selenium, tellurium and highly siderophile elements in the Earth's mantle: Evidence from mineral separates of ultra-depleted mantle residues. Chemical Geology, 396: 16-24.
Krot, A.N., Petaev, M.I., Scott, E.R.D., Choi, B.G., Zolensky, M.E., Kiel, K., 1998. Progressive alteration in CV3 chondrites: More evidence for asteroidal alteration. Meteoritics & Planetary Science 33, 1065-1085.
Kurzawa, T., König, S., Labidi, J., Yierpan, E., Schoenberg, R., 2017. A method for Se isotope analysis of low ng-level geological samples via double spike and hydride generation MC-ICP-MS. Chemical Geology https://doi.org/10.1016/j.chemgeo.2017.06.012.
Labidi, J., Farquhar, J., Alexander, C.M.O.D., Eldridge, D.L., Oduro, H., 2017. Mass independent sulfur isotope signatures in CMs: implications for sulfur chemistry in the early Solar System. Geochimica et Cosmochimica Acta 196, 326-350.
Larimer, J.W., 1968. An experimental investigation of oldhamite, CaS; and the petrological significance of oldhamite in meteorites. Geochimica et Cosmochimica Acta 32, 965-982.
Larimer, J.W., Ganapathy, R., 1987. The trace element chemistry of CaS in enstatite chondrites and some implications regarding its origin. Earth and Planetary Science Letters 84, 123-134.
Lauretta, D.S., Kremser, D.T., Fegley Jr, B., 1996. The rate of iron sulfide formation in the solar nebula. Icarus 122, 288-315.
Lehner, S.W., Petaev, M.I., Zolotov, M.Y., Buseck, P.R., 2013. Formation of niningerite by silicate sulfidation in EH3 enstatite chondrites. Geochimica et Cosmochimica Acta 101, 34-56.
Lodders, K., 2003. Solar System abundances and condensation temperatures of the elements. The Astrophysical Journal 591, 1220-1247.
Luck, J.-M., Othman, D.B., Albarede, F., 2005. Zn and Cu isotopic variations in chondrites and iron meteorites: Early solar nebula reservoirs and parent-body processes. Geochimica et Cosmochimica Acta 69, 5351-5363.

McEwing, C.E., Thode, H.G., Rees, C.E., 1980. Sulphur isotope effects in the dissociation and evaporation of troilite: a possible mechanism for 34S enrichment in lunar soils. Geochimica et Cosmochimica Acta 44, 565-571.
McSween, H.Y., Jr., 1977a. Carbonaceous chondrites of the Ornans type: A metamorphic sequence. Geochimica et Cosmochimica Acta 41, 477-491.
McSween, H.Y., Jr., 1977b. Petrographic variations among carbonaceous chondrites of the Vigarano type. Geochimica et Cosmochimica Acta 41, 1777-1790.
McSween, H.Y., Jr., Richardson, S.M., 1977. The composition of carbonaceous chondrite matrix. Geochimica et Cosmochimica Acta 41, 1145-1161.
Moynier, F., Blichert-Toft, J., Telouk, P., Luck, J.-M., Albarède, F., 2007. Comparative stable isotope geochemistry of Ni, Cu, Zn, and Fe in chondrites and iron meteorites. Geochimica et Cosmochimica Acta 71, 4365-4379.
Moynier, F., Paniello, R.C., Gounelle, M., Albarede, F., Beck, P., Podosek, F., Zanda, B., 2011. Nature of volatile depletion and genetic relationships in enstatite chondrites and aubrites inferred from Zn isotopes. Geochimica et Cosmochimica Acta 75, 297-307.
Pogge von Strandmann, P.A.E., Coath, C.D., Catling, D.C., Poulton, S.W., Elliott, T., 2014. Analysis of mass dependent and mass independent selenium isotope variability in black shales. Journal of Analytical Atomic Spectrometry 29, 1648.
Reisberg, L., Dauphas, N., Luguet, A., Pearson, D.G., Gallino, R., Zimmermann, C., 2009. Nucleosynthetic osmium isotope anomalies in acid leachates of the Murchison meteorite. Earth and Planetary Science Letters 277, 334-344.
Richter, F.M., Davis, A.M., 2004. Elemental and Isotopic Fractionation by Diffusion-limited Evaporation, Lunar and Planetary Institute Conference Abstracts, p. 2047.
Rouxel, O., Ludden, J., Carignan, J., Marin, L., Fouquet, Y., 2002. Natural variations of Se isotopic composition determined by hydride generation multiple collector inductively coupled plasma mass spectrometry. Geochimica et Cosmochimica Acta 66, 3191-3199.
Rubin, A.E., Trigo-Rodriguez, J.M., Huber, H., Wasson, J.T., 2007. Progressive aqueous alteration of CM carbonaceous chondrites. Geochimica et Cosmochimica Acta 71, 2361-2382.
Savage, P.S., Moynier, F., 2013. Silicon isotopic variation in enstatite meteorites: Clues to their origin and Earth-forming material. Earth and Planetary Science Letters 361, 487-496.
Schoenberg, R., Blanckenburg, F.v., 2006. Modes of planetary-scale Fe isotope fractionation. Earth and Planetary Science Letters 252, 342-359.
Schoenberg, R., Merdian, A., Holmden, C., Kleinhanns, I.C., Haßler, K., Wille, M., Reitter, E., 2016. The stable Cr isotopic compositions of chondrites and silicate planetary reservoirs. Geochimica et Cosmochimica Acta 183, 14-30.
Schönbächler, M., Rehkamper, M., Fehr, M.A., Halliday, A.N., Hattendorf, B., Gunther, D., 2005. Nucleosynthetic zirconium isotope anomalies in acid leachates of carbonaceous chondrites. Geochimica et Cosmochimica Acta 69, 5113-5122.
Simon, S.B., Grossman, L., Casanova, I., Symes, S., Benoit, P.H., Sears, D.W., Wacker, J.F., 1995. Axtell, a new CV3 chondrite find from Texas. Meteoritics 30, 42-46.
Tachibana, S., Huss, G.R., 2005. Sulfur isotope composition of putative primary troilite in chondrules from Bishunpur and Semarkona. Geochimica et Cosmochimica Acta 69, 3075-3097.
Trinquier, A., Elliott, T., Ulfbeck, D., Coath, C., Krot, A.N., Bizzarro, M., 2009. Origin of Nucleosynthetic Isotope Heterogeneity in the Solar Protoplanetary Disk. Science 324, 374-376.
Vollstaedt, H., Mezger, K., Leya, I., 2016. The isotope composition of selenium in chondrites constrains the depletion mechanism of volatile elements in solar system materials. Earth and Planetary Science Letters 450, 372-380.
Wang, Z., Becker, H., 2013. Ratios of S, Se and Te in the silicate Earth require a volatile-rich late veneer. Nature 499, 328-331.
Wasson, J.T., Isa, J., Rubin, A.E., 2013. Compositional and petrographic similarities of CV and CK chondrites: A single group with variations in textures and volatile concentrations attributable to impact heating, crushing and oxidation. Geochimica et Cosmochimica Acta 108, 45-62.
Young, E.D., Galy, A., Nagahara, H., 2002. Kinetic and equilibrium mass-dependent isotope fractionation laws in nature and their geochemical and cosmochemical significance. Geochimica et Cosmochimica Acta 66, 1095-1104.
Zahnle, K.J., Walker, J.C.G., 1982. The evolution of solar ultraviolet luminosity. Reviews of Geophysics 20, 280-292.
Zanda, B., 2004. Chondrules. Earth and Planetary Science Letters 224, 1-17.
Zanda, B., Hewins, R.H., Bourot-Denise, M., Bland, P.A., Albarède, F., 2006. Formation of solar nebula reservoirs by mixing chondritic components. Earth and Planetary Science Letters 248, 650-660.

762 Zanda, B., Yu, Y., Bourot-Denise, M., Hewins, R.H., Connolly, H.C., Jr., 1995. Sulfur behavior in
763 chondrule formation and metamorphism. Geochimica et Cosmochimica Acta, Submitted.
764 Zhang, X., Johnson, M., Koplitz, B., 2013. Using Anisotropy Measurements from A-Band
765 Photodissociation to Interrogate the Excited States of H2Se. journ. phys. chem. 117, 11963-11969.
766 Zhu, J.-M., Johnson, T.M., Clark, S.K., Zhu, X.-K., Wang, X.-L., 2014. Selenium redox cycling during
767 weathering of Se-rich shales: A selenium isotope study. Geochimica et Cosmochimica Acta 126, 228-
768 249.
769 Zolensky, M.E., Thomas, K.L., 1995. Iron and iron-nickel sulfides in chondritic interplanetary dust
770 particles. Geochimica et Cosmochimica Acta 59, 4707-4712.
771

Figure 1

Click here to download Figure: Fig 1.pdf

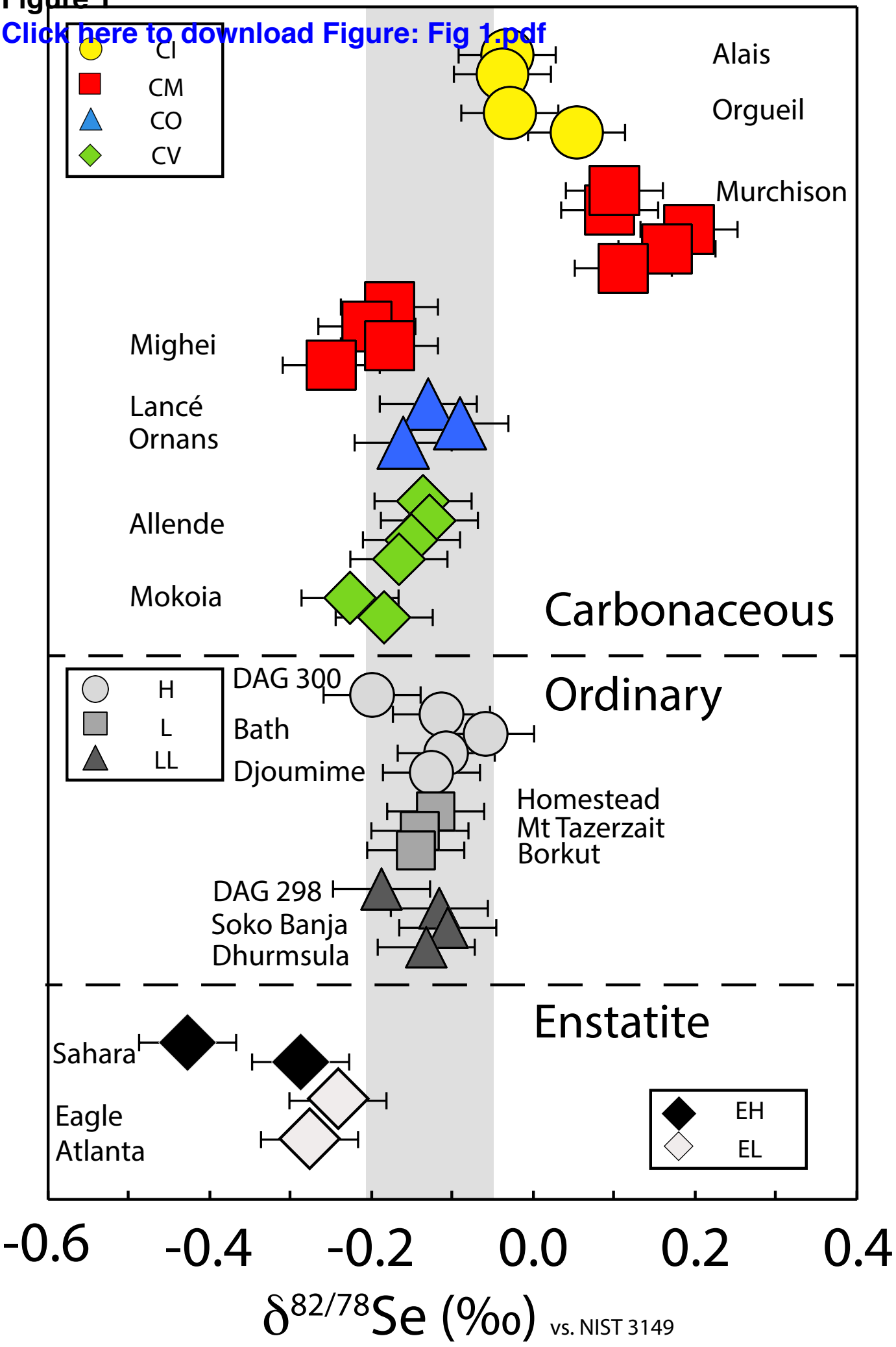

Figure 2
Click here to download Figure: Fig2 with ppm .pdf

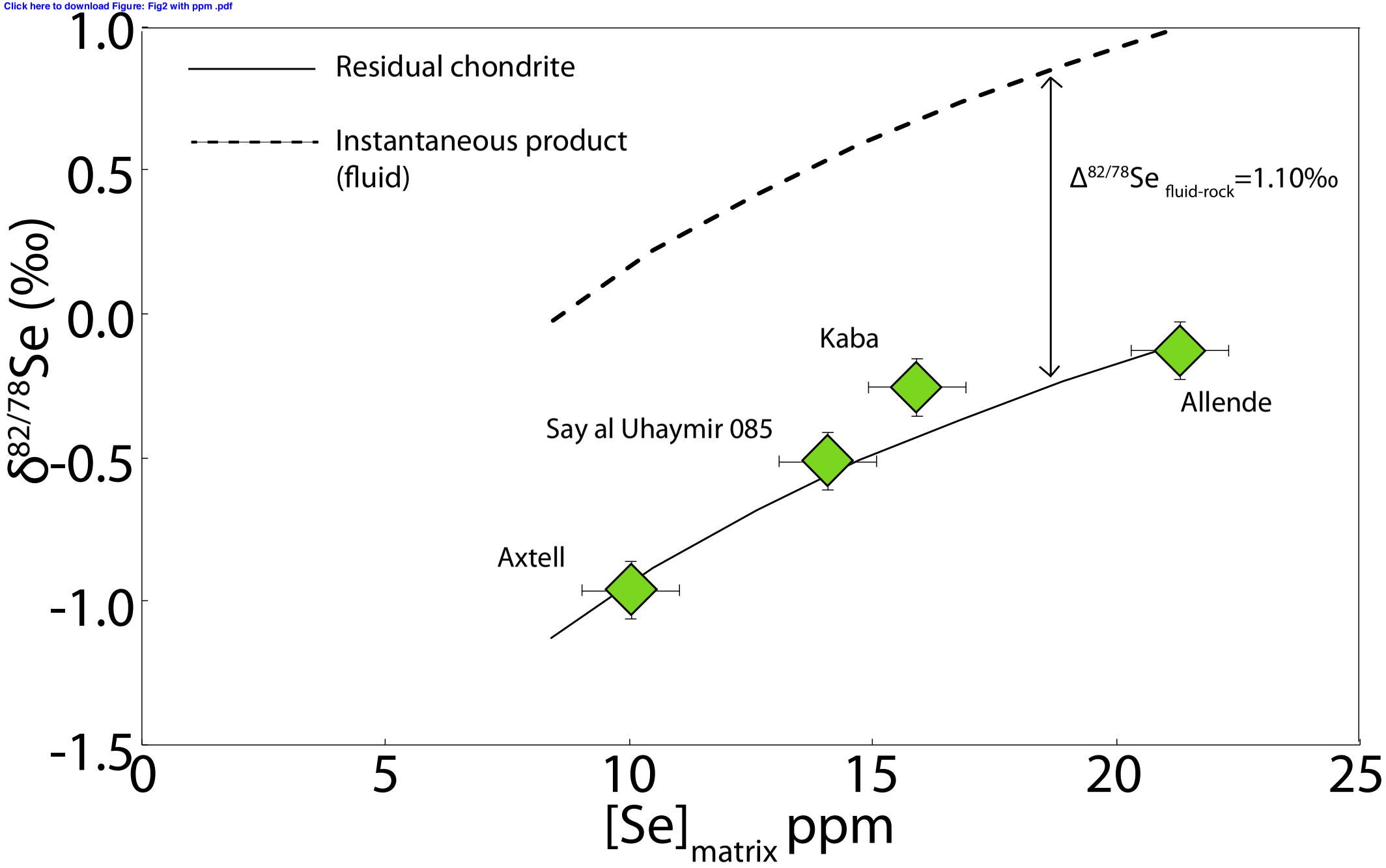

Figure 3

Click here to download Figure: Fig 3.pdf

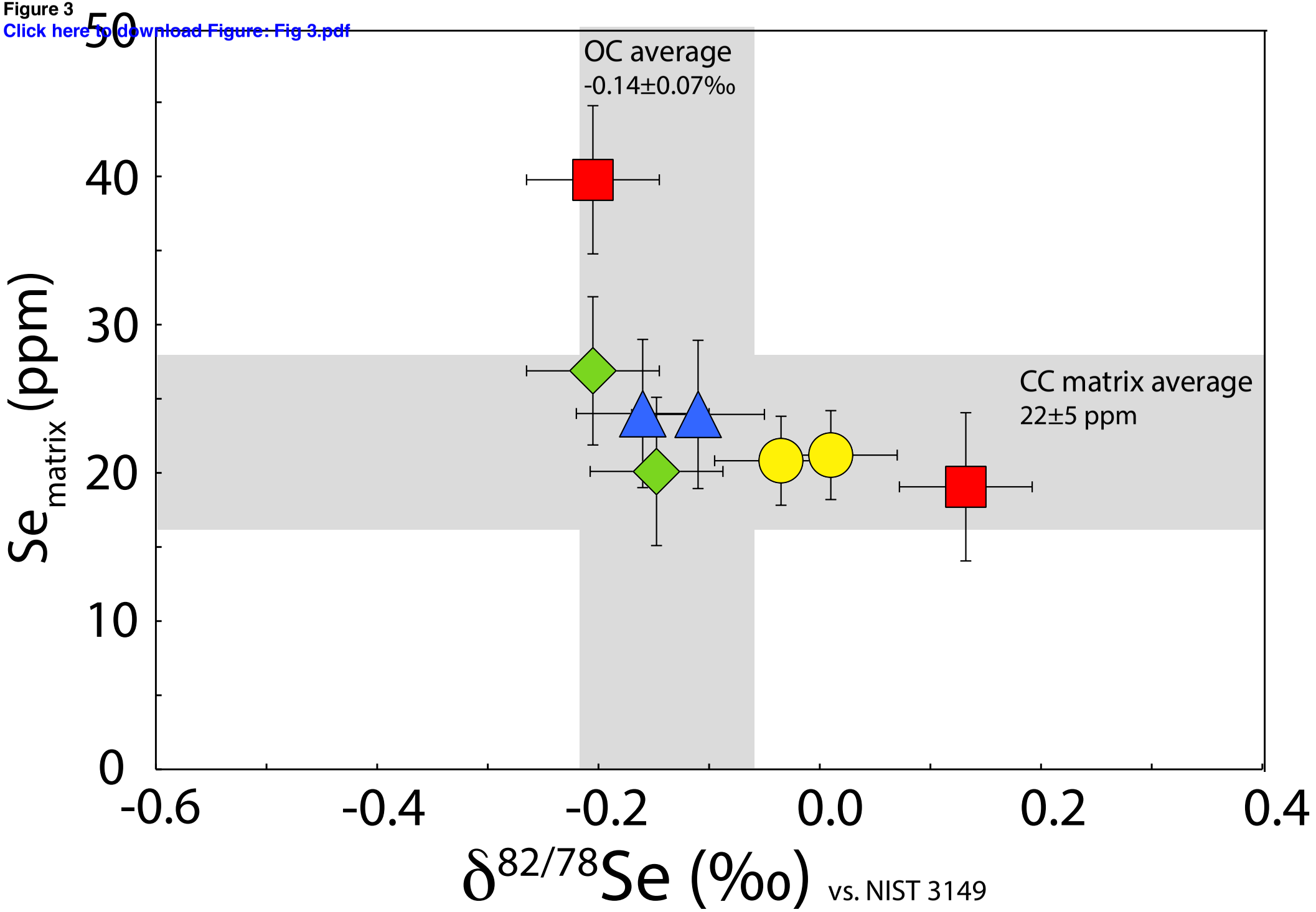

Figure 4

Click here to download Figure: Fig4.pdf

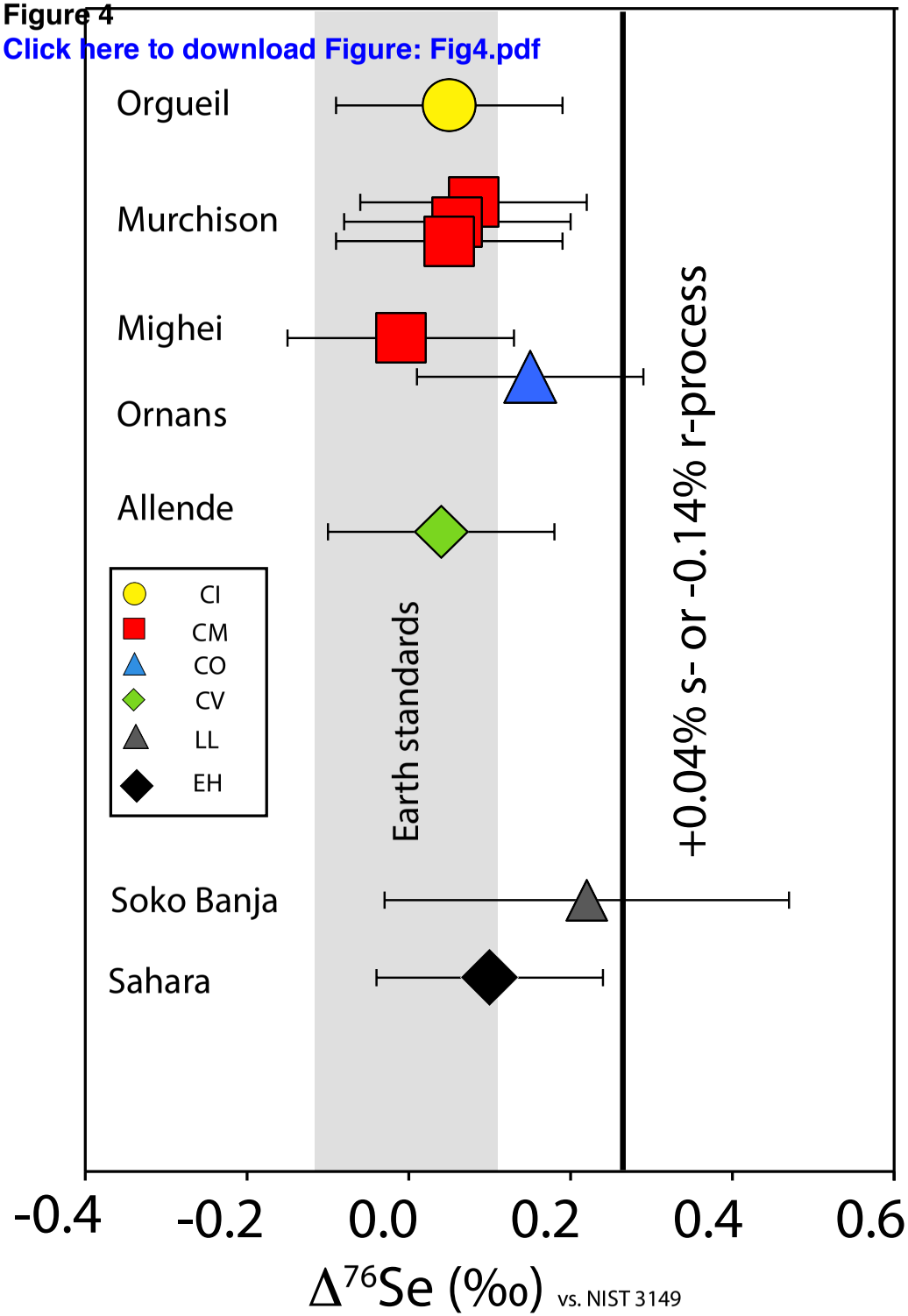

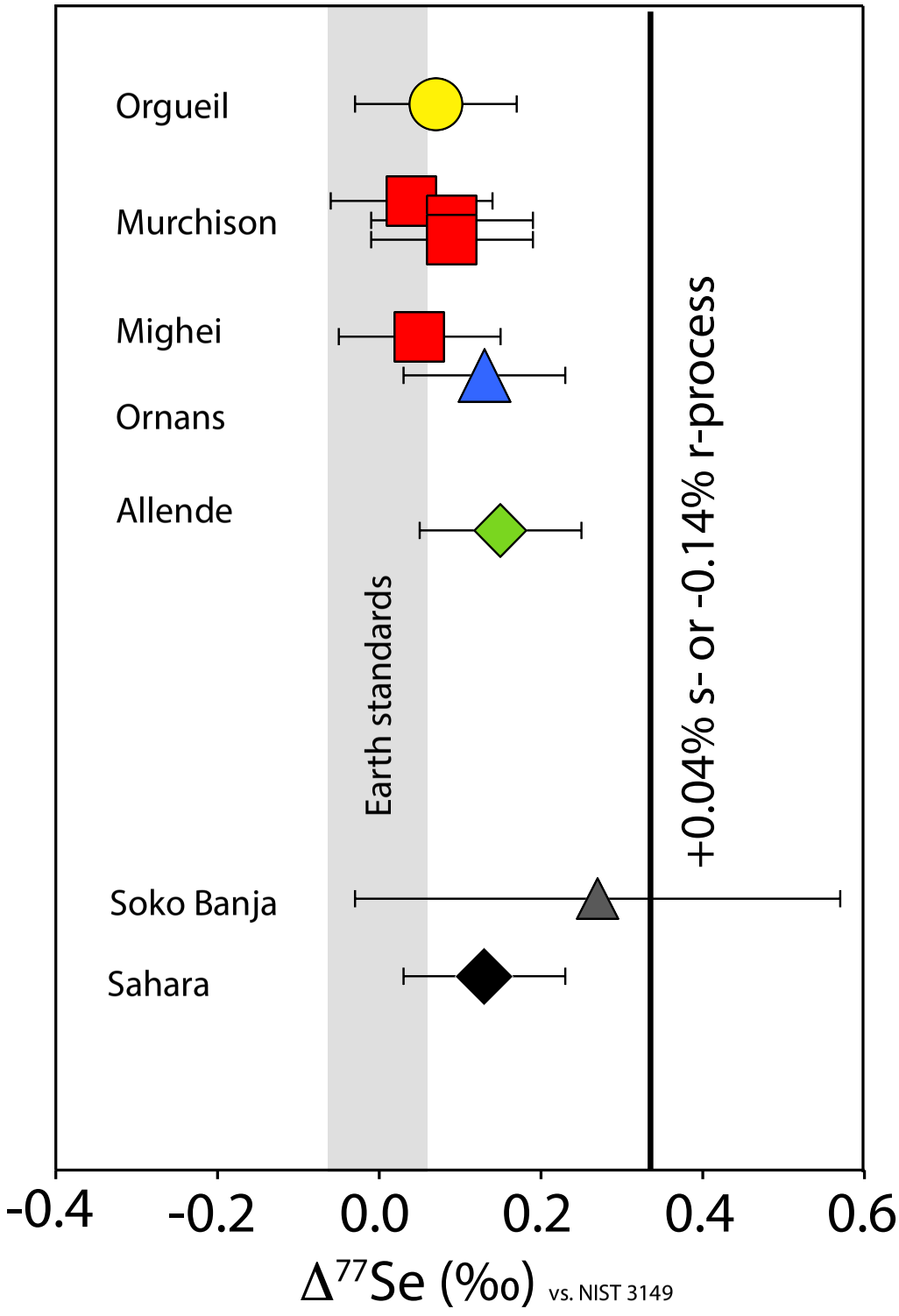

Table 1

Click here to download Table: Table 1 vfinal.xls

Table 1

Se content and isotopic data of meteorite aliquot obtained with the double spike method

sample type	Digestion temperature (°C)	amont digested (mg)	Aliquot ID	chondrite type	$\delta^{82/78}$Se (‰)	$[Se]_{bulk}$ (ppm)	$[Se]_{matrix}$ (ppm)
shale standard	220	11.9	SGR1		-0.14	3.9	
shale standard	220	11.9	SGR2		-0.06	3.6	
shale standard	220	13.4	SGR3		-0.12	3.3	
shale standard	220	66.4	SGR4		-0.09	3.2	
shale standard	220	74.3	SGR5		-0.06	3.5	
shale standard	220	92.5	SGR6		-0.18	3.5	
			average		**-0.11**	**3.5**	
fall	220	10.1	Alais 1	CI1	-0.03	21.7	
fall	220	3.9	Alais 2	CI1	-0.04	19.9	
			average		**-0.03**	**20.8**	20.8
fall	220	5.7	Orgueil 1	CI1	-0.03	21.5	
fall	100	24.3	Orgueil 2	CI1	0.05	20.9	
			average		**0.01**	**21.2**	21.2
fall	220	9.2	Mighei 1	CM2	-0.18	23.3	
fall	220	6.6	Mighei 2	CM2	-0.20	24.7	
fall	220	6.4	Mighei 3	CM2	-0.18	23.0	
	100	20.6	Mighei 4	CM2	-0.25	26.1	
			average		**-0.20**	**24.3**	39.8
fall	220	15.6	Murchison 1	CM2	0.09	13.4	
fall	220	12.9	Murchison 2	CM2	0.10	13.3	
fall	220	33.1	Murchison 3	CM2	0.19	12.2	
fall	220	26.8	Murchison 4	CM2	0.17	10.4	
	100	19.9	Murchison 5	CM2	0.11	11.7	
			average		**0.13**	**12.2**	19.1
fall	220	14.7	Allende 1	CV3 OxA	-0.13	8.0	
fall	220	11.2	Allende 2	CV3 OxA	-0.13	9.0	
fall	220	8.8	Allende 3	CV3 OxA	-0.15	8.6	
	100	36.8	Allende 4	CV3 OxA	-0.17	6.6	
			average		**-0.15**	**8.0**	20.1
fall	220	10.1	Mokoia 1	CV3 OxB	-0.22	10.8	
fall	220	6.6	Mokoia 2	CV3 OxB	-0.18	11.4	
			average		**-0.20**	**11.1**	26.9
fall	220	22.3	Kaba 1	CV3 OxB	-0.45	8.3	
fall	220	9.0	Kaba 2	CV3 OxB	-0.35	8.9	
			average		**-0.40**	**8.6**	16.2
find	220	16.8	Sayh al uha	CV3	-0.55	5.5	
find	220	15.8	Sayh al uha	CV3	-0.49	5.8	
			average		**-0.52**	**5.6**	12.8
find	220	15.6	Axtell 1	CV3 OxB	-0.94	4.0	
find	220	15.1	Axtell 2	CV3 OxB	-0.99	4.1	
			average		**-0.97**	**4.0**	10.0
fall	220	12.5	Ornans 1	CO3.4	-0.11	7.1	
fall	100	18.8	Ornans 2	CO3.4	-0.13	8.6	
			average		**-0.12**	**7.9**	18.3
fall	220	17.3	Lancé	CO3.5	-0.16	8.4	24.0
find	100	15.0	Sahara 970	EH3	-0.43	22.1	
	220	6.2	Sahara 970	EH3	-0.29	18.5	
			average		**-0.36**	**20.3**	
fall	220	9.6	Eagle	EL6	-0.24	10.0	
fall	220	9.6	Atlanta	EL6	-0.28	9.0	
find	220	26.3	Dar Al Gani	H3-5	-0.20	8.0	
fall	100	19.2	Bath 3	H4	-0.11	6.5	
fall	220	36.6	Bath1	H4	-0.06	8.0	
fall	220	36.0	Bath2	H4	-0.11	7.9	
			average		**-0.09**	**7.5**	
fall	220	19.1	Djoumine	H5-6	-0.13	9.2	
fall	220	10.5	Homestead	L5	-0.12	8.7	
fall	220	10.6	Mt Tazer	L5	-0.14	8.8	
fall	220	29.9	Borkut	L5	-0.15	9.6	
find	220	11.5	Dar Al Gani	LL4	-0.19	5.9	
fall	220	48.6	Soko Banja	LL4	-0.12	6.8	
fall	100	20.4	Soko Banja	LL4	-0.11	7.1	
			average		**-0.11**	**7.0**	
fall	220	30.5	Dhurmsala	LL6	-0.13	9.8	

Table 2
Click here to download Table: Table 2.xlsx

Table 2
Se isotopic data of meteorite aliquot obtained with the sample-standard bracketing method.
See table 1 for corresponding d82/78Se value obtained with the double-spike technique.
Internal uncertainties in 2 s.d. are 0.2‰ for $\delta^{82/78}$Se, 1.5‰ for Δ^{74}Se, 0.14‰ for Δ^{76}Se and 0.10‰ for Δ^{77}Se.
For soko Banja and Ornans, uncertainties were higher (see text) due to low Se amount available for analysis
For a given aliquot, $\delta^{82/78}$Se obtained with standard-sample bracketing measurements were 0.7‰ higher on average than with the double spike approach. This is because the solutions experienced 5-30% Se evaporative loss as described in Kurzawa et al. (2017). While by design, such fractionations are corrected by the double-spike deconvolution, they are observed with the standard-bracketing approach. Since evaporative fractionations are mass-dependent, we only discuss the mass-independent variations of ^{74}Se, ^{76}Se and ^{77}Se at a given ^{82}Se/^{78}Se ratio, quantified as Δ^{74}Se, Δ^{76}Se and Δ^{77}Se in per mil (see equation 4).

	$\delta^{82/78}$Se	$\delta^{74/78}$Se	$\delta^{76/78}$Se	$\delta^{77/78}$Se	Δ^{74}Se	Δ^{76}Se	Δ^{77}Se
MH-954	-2.10	2.42	1.01	0.59	0.1	-0.12	0.03
MH-954	-2.11	2.40	1.03	0.56	0.1	-0.11	0.00
MH-954	-2.11	2.34	1.14	0.57	0.0	0.00	0.01
MH-954	-2.12	2.30	1.14	0.54	-0.1	-0.01	-0.02
soko banja 2	0.83	-0.64	-0.23	0.05	0.3	0.22	0.27
sahara 2	0.21	-0.86	-0.01	0.07	-0.6	0.10	0.13
Mighei 4	0.08	-0.77	-0.05	0.03	-0.7	-0.01	0.05
Ornans 2	1.22	-0.10	-0.51	-0.19	1.3	0.15	0.13
orgueil 2	-0.03	0.86	0.07	0.08	0.8	0.05	0.07
Allende 4	0.86	0.19	-0.42	-0.08	1.1	0.04	0.15
Murchison 5	0.53	-0.41	-0.24	-0.05	0.2	0.05	0.09
Murchison 3	0.22	-0.33	-0.04	-0.02	-0.1	0.08	0.04
Murchison 4	0.17	-0.09	-0.03	0.04	0.1	0.06	0.09

Supplementary material for online publication only

Click here to download Supplementary material for online publication only: Supplementary information-V2.docx

Fig S1

Click here to download Supplementary material for online publication only: Fig S1-true.pdf